Analysis and Optical Characterisation of Bolometric Integrating Cavities Including a Free Space Gap in the Waveguide Structure

Darragh McCarthy[1], Neil Trappe[1], Stephen Doherty[1], J. Anthony Murphy[1], Colm Bracken[1], Marcin Gradziel[1], Créidhe O'Sullivan[1], Maarten van der Vorst[2], Michael D. Audley[3], Gert de Lange[3]
[1]Maynooth University Department of Experimental Physics, Maynooth University, Maynooth, Ireland,
darragh.mccarthy@nuim.ie
[2]European Space Research and Technology Centre (ESTEC), ESA, Noordwijk, Netherlands
[3]Space Research Organisation of the Netherlands (SRON), Groningen, Netherlands

***Abstract*—Bolometric integrating cavities have been used with great success in previous far-infrared space missions, and are planned for extensive use in future missions where ever increasing sensitivity is required. It is critical for the purposes of design and the interpretation of results that these systems are thoroughly understood and optically characterised fully. Such systems, for manufacturing and mechanical reasons, may contain free space gaps between the feed horn antenna and the integrating cavity, and so it is necessary to include the effect of these waveguide openings in simulations. Since these pixels are electrically large, it is more feasible to model them by using the computationally efficient mode-matching approach. In this paper we discuss the elements required to model such pixels within the mode-matching approach and apply it to a typical pixel containing a free space gap, based on an experimental Transition Edge Sensor (TES) cavity waveguide pixel at SRON Groningen.**

***Index Terms*—multi-moded, mode matching, free space, bolometer, integrating cavity, Transition Edge Sensor.**

I. Introduction

In future far-infrared space based systems, an increase in sensitivity is required. This will be achieved by using a greater number of detectors packed densely in a focal plane area. Such pixels can also be multi-moded across the bandwidth of interest, resulting in increased throughput to the detectors. An example of such a system is the SAFARI instrument onboard the proposed SPICA mission. Future Cosmic Microwave Background (CMB) missions will also require a large number of detectors and will potentially use a superconducting bolometer in a waveguide structure. Pixels for missions of this type may typically consist of a multi-moded horn antenna that feeds an integrating cavity that contains an absorbing superconducting layer which is used, in the case of SAFARI, with a Transition Edge Sensor (TES) coupled bolometer in order to measure the absorbed power. For mechanical reasons, a gap exists in such systems between the horn antenna and the cavity containing the detector to mechanically allow the separate manufacture of the horn and cavity arrays. This is because the horn antennas forming the input to the detector array are wire cut from a solid metal block, and the detector array is manufactured on silicon wafer. Since these two sections cannot be pressed together, and since the absorber must sit slightly outside the cavity, there is a gap. The gap in such systems serves a second purpose, namely to introduce sufficient separation between the horns and cavities/detectors so that the vibrations induced at launch do not result in them contacting each other and causing damage.

In order to be able to design and optimise pixels such as these for use in future missions, it is necessary to include them in the design process so as the full performance of each pixel can be assessed, including power leakage. Full electromagnetic solvers such as Computer Simulation Technology Microwave Studio (CST MWS) and COMSOL are capable of predicting the performance of such structures, however pixels such as the ones under consideration are electrically large. Given the computing resources typically available, simulations in these packages often cause the available memory to be exceeded or take several days to complete. Reliable modelling techniques must be available to design and improve such pixels (perhaps by using an optimisation algorithm), so it is clear that a more efficient technique must be used. The mode matching technique offers a significantly more efficient approach. allowing a complete description of the horn and cavity structures that are used, along with the absorber which is modelled as an ohmic sheet. In order to fully implement such a pixel using this technique, it is necessary to account for the effects of the free space gap and the resulting metal face presented by the block that the horn antennas are cut from, as in figure 1. As a first approximation it is possible to include the gap as a section of waveguide of large radius, however the number of waveguide modes necessary to do this (see section II) would be computationally prohibitive. In this paper, these elements will be integrated with the standard mode matching technique in order to completely model such pixels. The performance of the technique will be verified using a commercial electromagnetic solver and then applied to a system based on an experimental test bed at Space Research Organisation of the Netherlands (SRON) Groningen, which includes a gap that approximates to free space.

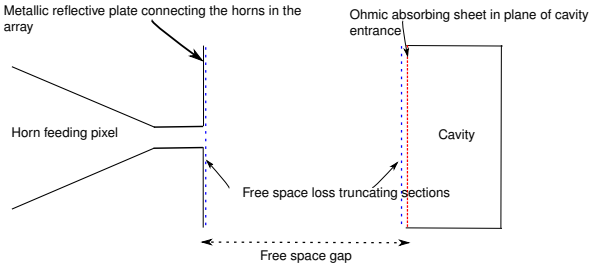

Fig. 1. Schematic of an example of the pixels in question

II. Implementing the Gap

The geometry of the pixels in question is assumed to by cylindrical. Software developed at Maynooth University, known as SCATTER, is capable of modelling such structures by means of the mode matching technique [1]. This technique functions by expressing a waveguide structure such as horn antenna or a cavity as a series of sections, where the radius of each section is different to that of the sections either side. By expressing the field in each section using a suitable number of transverse electric (TE) and transverse magnetic (TM) waveguide modes, a set of scattering matrices can be found that govern the behaviour of that section in terms of bi-directional transmission and reflection. These matrices transform the coefficients of each mode at the input of that section to the output, accounting for the affect of the section. By calculating the scattering matrices associated with each section and cascading them sequentially, a set of scattering matrices can be found which relate the input of the overall system to the output. In order to incorporate additional elements within SCATTER (such as those shown in figure 1, for example the elements required to implement the free space gap), a set of scattering matrices must be found that describe such elements. These scattering matrices can then be included at the appropriate points in the calculation in order to include the effect of the additional sections. In this section, the required scattering matrices will be discussed and derived.

A. Transition from Waveguide Modes to Free Space Modes

In SCATTER, the electric and magnetic field components in each waveguide section are represented by sums of Transverse Electric (TE) and Transverse Magnetic (TM) modes, [1], with the field at the exit interface to free space of the structure therefore represented in terms of these modes. The mathematical form of these modes is presented in [3]. In order to propagate the field from the exit aperture through free space to some plane of interest, it is necessary to transform the field at the aperture so as it is represented using a basis set that is representative of free space fields. Assuming a cylindrically symmetric system geometry, the most natural mode set to select is the Associated Laguerre Gaussian (LG) mode set, [2]. This mode set is the solution to the Helmholtz equation in the paraxial limit, with the LG modes of order m and degree α given by

$$\begin{pmatrix} \Psi_m^{\alpha,\cos}(r,\phi,z) \\ \Psi_m^{\alpha,\sin}(r,\phi,z) \end{pmatrix} = \sqrt{\frac{2(2-\delta_{0\alpha})\,m!}{\pi W^2 (m+\alpha)!}} \exp\left(\frac{-r^2}{W^2}\right) \times \left(\frac{2r^2}{W^2}\right)^{\frac{\alpha}{2}} L_m^{\alpha}\left(\frac{2r^2}{W^2}\right) \exp\left(-jk\left(\frac{r^2}{2R}\right)\right) \times \exp\left(-j\left(kz - \phi_{m,\alpha(z)}\right)\right) \begin{pmatrix} \cos\alpha\phi \\ \sin\alpha\phi \end{pmatrix}, \quad (1)$$

where $L_m^{\alpha}(x)$ are the Associated Laguerre polynomials of order m and degree α. W, R and $\phi_{m,\alpha}$ are the width, phase radius of curvature and the phase slippage of each mode, each being a function of the distance propagated from the beam waist, the point at which the beam has minimum width. These parameters are defined fully in [2]. This allows the expression of any cylindrical field E in terms of this mode set according to

$$E(r,\phi,z) = \sum_{\alpha,m}^{N} A_{\alpha,m}\Psi_m^{\alpha\cos}(W,R,r,\phi,z) + \sum_{\alpha,m}^{N} B_{\alpha,m}\Psi_m^{\alpha\sin}(W,R,r,\phi,z), \quad (2)$$

where $A_{\alpha,m}$ and $B_{\alpha,m}$ are the coefficients of each mode, found by carrying out an overlap between each mode and E in the plane where the transition between the mode sets is occurring.

As outlined in [3], it is possible to take a field represented by waveguide modes and couple it to the free space modes. For waveguide modes of azimuthal order n, only coupling to LG modes of degree $n \pm 1$ need be considered. Where $n = 0$, only coupling to LG modes of degree 1 is necessary, as negative degrees are physically meaningless. Thus, for a given azimuthal order, a scattering matrix $T^{(n)}$ can be generated which relates each of the waveguide modes in that azimuthal order to the LG modes that are being coupled to. The entries in each of these matrices are found by carrying out an overlap integral between the waveguide modes and the free space modes. It should be noted that in systems which include the orthogonal polarisations of the waveguide modes, the coupling of these modes is the same and so does not need to be calculated separately. In order to couple back into the waveguide modes from free space, a similar process is carried out, with the waveguide modes now being conjugated in the overlap integral, as these are the modes being coupled into. This calculation can be eliminated by noting that the conjugate transpose of the transmission matrix T, gives the coupling of the free space modes back into the waveguide modes across the same transition aperture. This matrix is known as R, with $R_{i,j}^{(n)} = T_{i,j}^{(n)*}/|Z|$, where $|Z| \approx Z_0$, and Z_0 is the impedance of free space. The factor of Z appears in order to keep the normalisation consistent between the mode sets, as SCATTER assumes normalisation with respect to complex power. In this way, the set of scattering matrices governing any section that

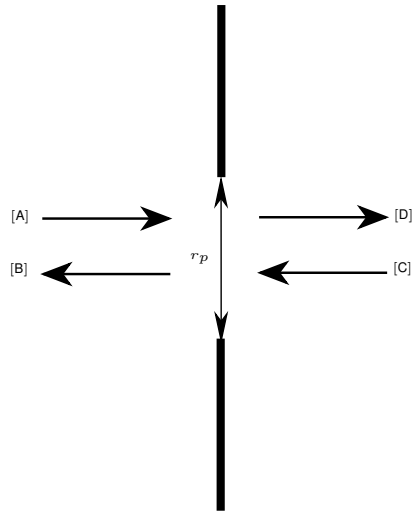

Fig. 2. Free space loss truncating section, simulating power loss beyond pixel extent

acts as an interface between free space and waveguide modes can be calculated such that $S_{21}^{i,j} = T_{i,j}$, $S_{12}^{i,j} = R_{i,j}$, $S_{11}^{i,j} = 0$ and $S_{22}^{i,j} = 0$.

B. Propagation Through Free Space

The field at the plane that interfaces between the mode sets, in terms of free space modes, can be written as

$$E_{in} = \sum_n A_n \Psi_n \left(W_{in}, R_{in}, \phi_{in}\right), \tag{3}$$

assuming n free space modes. The field at some output plane a distance z away can be computed by applying the ABCD matrix technique, [2], in order to calculate the values of the previously outlined beam parameters at the output plane, namely W_{out}, R_{out} and ϕ_{out}. This allows the field at the output plane to be reconstructed according to

$$E_{out} = \sum A_n \Psi_n \left(W_{out}, R_{out}, \phi_{out}\right), \tag{4}$$

where the mode coefficients, A_n, remain unchanged.

C. Free Space Loss Truncating Section

Power is conserved within the mode matching technique, so a power loss mechanism must be introduced across the free space gap. As a free space beam propagates, it increases in off-axis extent due to diffraction. For a given pixel radius, r_p, it is possible that the beam associated with certain free space modes may extend beyond this value. This power is lost from the pixel, and so should be quantified as when arrays are used it could result in crosstalk. To do this, it is necessary to truncate the free space modes beyond the spatial extent of the pixel. Figure 2 illustrates the method used to implement this, which is by means of a circularly symmetric sheet which is infinitely thin and perfectly absorbing, with a pupil of radius r_p centred on the optical axis of the system. The free space modes can travel either forward or backwards, where in figure 2, left to right is taken as the forward direction. Applying the mode matching technique [1] to this system, and assuming a total of N free space modes, the scattering matrices for this section are found to be

$$\begin{aligned} S_{11} &= 0 \\ S_{12} &= P_2 \\ S_{21} &= P_1 \\ S_{22} &= 0, \end{aligned} \tag{5}$$

where

$$P_1 = \int_0^{r_p} e_n^+ \cdot e_n^+ 2\pi r \mathrm{d}r, \tag{6}$$

and

$$P_2 = \int_0^{r_p} e_n^- \exp\left(\frac{jkr^2}{2R}\right) \cdot e_n^- 2\pi r \mathrm{d}r. \tag{7}$$

The P_n integrals represent the coupling of each through the pupil. As such, they represent the transmission of each mode through the truncating section. Since the reflection scattering matrices evaluate to zero, the balance of the power is considered to be lost from the pixel through the gap.

D. Horn Array Reflective Plate

Figure 1 shows a schematic of the overall pixel being simulated. The pixel will ultimately be a part of an array, with the horn for each pixel being drilled into one large plate of metal (this study is based on a single pixel prototype and so one pixel is considered in isolation). It is clear from the schematic that the pixel encompasses a part of this plate which behaves as a reflective surface whose impact must be accounted for in simulations. To implement this plate within the mode matching framework, it is assumed that the gap is being fed by a waveguide aperture of radius a, as in figure 3. In the limit that $\delta \to 0$, the reflective plate is in contact with the waveguide, as in the pixel. In this case, no radiation incident upon the sheet from the left exists beyond a distance a off-axis, so $[A]$ and $[B]$ exist only in the region $r < a$. To implement the reflective plate, the waveguide modes at the waveguide aperture are transformed into free space modes, and these modes are immediately applied to the plate. If the plate is assumed to be infinitely thin, then this process results in the modes propagating a zero distance in free space, with the plate effectively truncating the free space field. Using these assumptions and applying the mode matching technique yields the following scattering matrices for the plate,

$$\begin{aligned} S_{11} &= 0 \\ S_{12} &= P_2 \\ S_{21} &= P_1 \\ S_{22} &= -Q_2, \end{aligned} \tag{8}$$

where the P_n integrals are as before, and $Q_2 = \int_{r_p}^{\infty} e_n^- \exp\left(\frac{jkr^2}{2R}\right) \cdot e_n^+ 2\pi r \mathrm{d}r$, represents the reflection coefficients on the free space side of the plate.

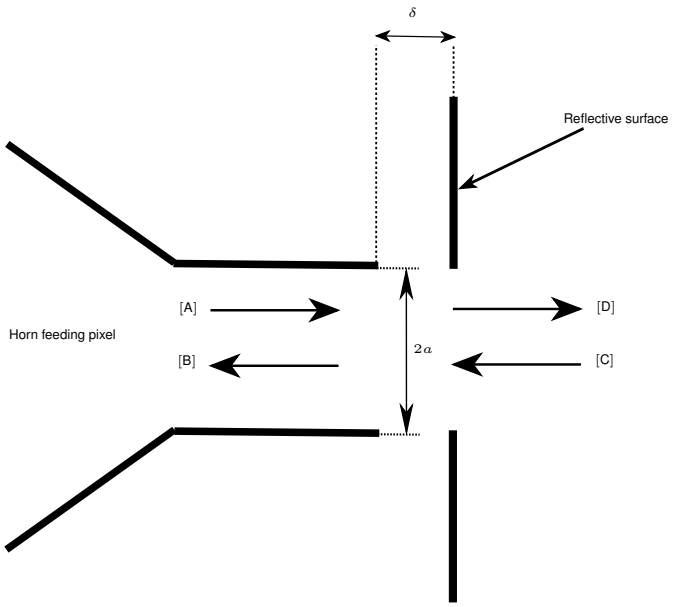

Fig. 3. Reflective plate section in the mode matching technique

III. Verification and Application to a Test Pixel

By implementing an electrically small single-moded waveguide (r=1.535 mm) fed cavity structure (r=2 mm) in CST, it was possible to verify the correct performance of the elements described above. At a frequency of 70 GHz, this structure was simulated for varying values of the gap between the waveguide and the cavity, with the power leaking from the structure recorded using a field monitor. The same system was implemented in SCATTER, with the leaked power being monitored by performing a singular value decomposition (SVD) on the S_{11} matrix of the system. Since this is the only port for power to enter/exit the system, and the only loss mechanism is the gap, then any power that does not return to port 1 must have been lost to the gap. The leaked power was thus evaluated according to

$$P_{\text{leaked}} = \sum_{1}^{\beta} i - \sum_{i}^{\beta} \sigma_i^2. \tag{9}$$

where σ_i is the singular value of the i^{th} mode supported by the system and $i = 1$ for a single-moded system.

Figure 4 compares the leaked power predicted by both methods. For a given frequency, larger gaps result in more power being lost due to each mode diffracting to a larger degree. The disagreement for lower gap lengths is expected. For small distances the system is in the reactive nearfield, whose affects are not accounted for in the mode matching technique. This work is focussed on pixels in which the wavelength varies from 35 to 70 μm with a gap of length 50 μm. This corresponds to gap lengths (in terms of λ) of $\approx 0.71 - 1.42$ λ. Figure 4 shows excellent agreement when the length of the gap is of this order, and so the SCATTER approach can be applied with confidence to such pixels. The CST simulations took several hours to run, with SCATTER

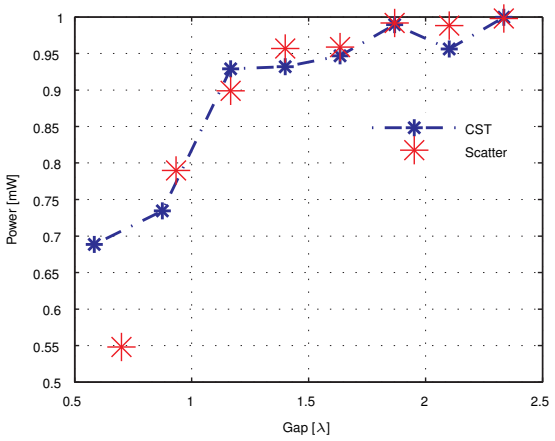

Fig. 4. Comparison of leaked power as a function of free space gap length (expressed in terms of wavelength ($\lambda = 4.28275\text{mm}$)) found using CST and SCATTER

TABLE I
Details of the various pixel configurations simulated

Configuration	D_{BB} [mm]	L_{BB} [mm]
1	13.00	26.10
2	0.90	10.77
3	0.50	10.20
4	1.40	10.20

taking less than an hour. This shows the improved efficiency that is obtained using the mode matching technique.

The pixel design that will be analysed is based on an experimental arrangement of a pixel at SRON Groningen, which is a prototype of a SAFARI pixel. The prototype pixel is of cylindrical geometry, with a smooth-walled conical horn of throat radius 23 μm feeding a hemispherical backshort cavity containing a TES device with an entrance aperture radius of 250μm via a gap of 50μm. In the measurement setup, a conical radiator is used to illuminate the pixel. The radiator illuminates a pinhole aperture of radius D_{BB} with the pixel entrance aperture located a distance L_{BB} from this. The pixel was illuminated using this source for various combinations of D_{BB} and L_{BB}, as shown in table I. By simulating the pixel in SCATTER and performing a SVD on the S_{11} matrix, the modes supported by the system can be identified. These modes are then coupled to the conical radiator, modelled as blackbody source, and the amount of each mode that actually gets excited in the pixel is recovered as a percentage of the amount of power that was available to that mode. Thus, the figure returned for lost power is the power lost as a percentage of the power that was available to couple to the pixel.

Three pixel models were considered for each configuration, a closed pixel (no gap) with just an ohmic sheet to model the bolometer absorber, an open pixel (gap included) with no absorber and an open pixel with an absorber, i.e. the full pixel. The total lost power as a fraction of the total power available to the pixel was calculated across the band from 35-70 μm in 53 steps for each configuration, with the results shown in figure 5. Configuration 1 corresponds to a pinhole aperture

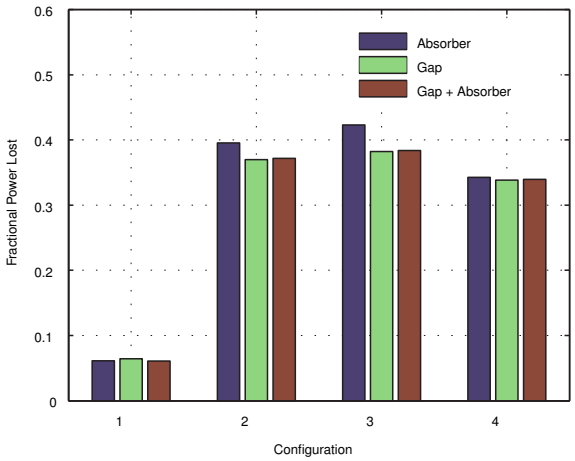

Fig. 5. Comparison of the integrated fractional power lost for each configuration for three pixel models

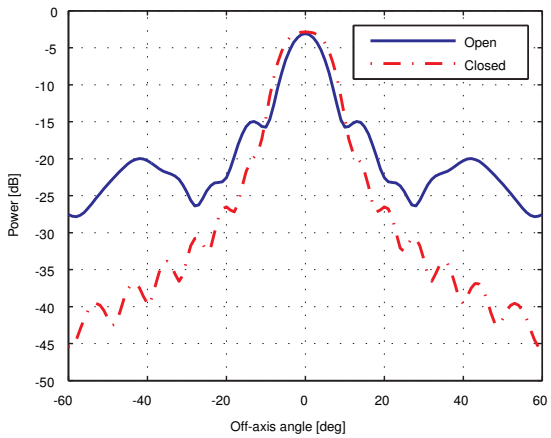

Fig. 6. Farfield beam patterns for open and closed pixels at λ =50 μm

that is sufficiently large to be invisible to the pixel, thus the pixel sees the blackbody source directly. Since this is highly non-directional, the coupling of the pixel to this source is low, hence the low value for efficiency. The results for the other configurations, which yield usable source beams, show that for a closed cavity with an absorber the highest amount of power is lost. The least amount of power is lost when an empty, open pixel is considered. When both mechanisms are combined, the figure obtained is slightly higher than the empty, open pixel, but less than the closed pixel with the absorber. The result of combining both mechanisms should not be expected to be a linear combination of the losses due to both mechanisms individually, as the electromagnetic system in question is fundamentally different, so this result is expected.

The reduced fraction of lost power that is observed when both mechanisms are combined (relative to the closed pixel) can be considered by examining the farfields of the open and closed pixels (both with absorbers). A comparison between the two for λ =50 μm is shown in figure 6, with a similar situation occurring across the band. Due to increased reflections and back scattering introduced by the free space gap, more modes are supported by the open pixel than the closed pixel at a given wavelength. This results in the farfield beam pattern of the open pixel containing a higher percentage of off-axis power than the corresponding closed pixel. This reduces the directivity of the beam, and since the source being coupled to is aligned with the optical axis of the pixel, the coupling reduces, resulting in less leaked power. This analysis was previously not possible to carry out using CST (owing to memory requirements), and so the mode matching technique has allowed additional insight to be gained into the performance of the pixel.

IV. Conclusion

The gap present in the SAFARI pixel for mechanical reasons was modelled as a free space gap, and the elements required to model this gap as an integrated part of the mode matching technique were presented and implemented. The resulting model was tested against a waveguide fed cavity using CST MWS, with excellent agreement being observed for sufficiently large values of the gap in terms of wavelength, once the reactive nearfield was exited. The range of effective gap values giving good agreement coincides with the effective gap lengths encountered in the systems of interest in this work. A pixel, as implemented at SRON Groningen, was then modelled with the gap included, and the results obtained were compared to a closed pixel and an open pixel with no absorber, in order to illustrate the effect of including the gap. The results were found to be consistent with the expected behaviour of the system and showed that including the gap has a small but visible impact on the total power removed from the pixel by the combination of the gap and the absorbing sheet in the cavity associated with the measurement system. It was noted during the various simulations that the run time required when using the mode matching technique was significantly less than when CST was used (less than an hour versus several hours), and no memory issues were encountered, allowing an analysis of the full pixel, including the free space gap.

Acknowledgments

The author wishes to acknowledge the financial support of the European Space Agency (ESA) and the Irish Research Council (IRC) EMBARK postgraduate scholarship scheme.

References

[1] A.D. Olver, P.J.B. Clarricoats, A.A. Kishk and L. Shafai, *Microwave Horns and Feeds*, IEEE Press, 1994.

[2] P.F. Goldsmith, *Quasioptical Systems-Gaussian Beam Quasioptical Propagation and Applications*, IEEE Press, 1998.

[3] N. Trappe, J.A. Murphy, S. Withington and W. Jellema, *Gaussian Beam Mode Analysis of Standing Waves Between Two Coupled Corrugated Horns*, IEEE TRANSACTIONS ON ANTENNAS AND PROPAGATION (53), No. 5, 2005.